

Towards a Complete Picture of Covariance Functions on Spheres Cross Time

Philip White¹ and Emilio Porcu²

¹Department of Statistical Science, Duke University, P.O. Box 90251, Durham, NC 27708, U.S.A.

²Chair of Spatial Analytics Methods. School of Mathematics and Statistics, Newcastle University, Newcastle upon Tyne, NE1 7RU. U.K.

June 15, 2022

Abstract

With the advent of wide-spread global and continental-scale spatiotemporal datasets, increased attention has been given to covariance functions on spheres over time. This paper provides a characterization theorem for covariance functions of random fields defined over d -dimensional spheres cross time. The result characterizes the relationship between covariance functions for spheres over time and space-time covariance functions defined over Euclidean spaces. We then show that the Gneiting class of space-time covariance functions (Gneiting, 2002) can be extended to spheres cross time by replacing the squared Euclidean distance with the great circle distance. Additionally, we provide a new class of covariance functions using our characterization theorem, giving an example of a class correspondence between covariance functions over Euclidean spaces with compact support and covariance functions over spheres cross time.

We discuss modeling details using nearest-neighbor Gaussian processes in a Bayesian framework for our extension of the Gneiting class. In this context, we illustrate the value of our proposed classes by comparing them to currently established nonseparable covariance classes using out-of-sample predictive criteria. These comparisons are carried out on a simulated dataset and two climate reanalysis datasets from the National Centers for Environmental Prediction and National Center for Atmospheric Research. In our simulation study, we establish that covariance parameters from a generative model from our class can be identified in model fitting and that predictive performance is as good or better than competing covariance models. In our real data examples, we show that our covariance class has better predictive performance than competing models, and we discuss results in the context of the climate processes that we model.

Keywords: Bayesian statistics; Covariance Functions; Global Data; Great Circle Distance; Spatiotemporal statistics; Sphere.

1 Introduction

In recent years, there has been a sharp increase in the prevalence of global or continental-scale spatiotemporal data due to satellite imaging, climate reanalyses, and wide-spread monitoring networks. Although Earth is not exactly spherical (it flattens at the pole), it is commonly believed that the Earth can be well approximated by a sphere (Gneiting, 2013; Castruccio & Stein, 2013). With the goal of modeling data over large spatial scales, while accounting for the geometry of the Earth, there has recently been fervent research on modeling and inference for random fields on spheres as well as on spheres cross time. Recent examples include Gneiting (2013); Jeong & Jun (2015); Porcu et al. (2016); Berg & Porcu (2017), and Porcu et al. (2018) give a comprehensive overview of these topics.

Under Gaussianity, the covariance function is core to spatiotemporal modeling, inference, and prediction. Covariance functions are positive definite, a property that requires non-standard mathematical tools from harmonic analysis to show. Following the works of Schoenberg (1942) and Gneiting (2013) on spheres, the mathematical characterization of covariance functions on spheres cross time has been given by Berg & Porcu (2017). In addition, Porcu et al. (2016) provide examples of covariance functions for practitioners. Generalizations in the area of mathematical analysis include Guella et al. (2016a,b, 2017) and Barbosa & Menegatto (2017).

For a random field on $\mathbb{R}^d \times \mathbb{R}$ with stationary covariance function $C : \mathbb{R}^d \times \mathbb{R} \rightarrow \mathbb{R}$, Gneiting (2002) showed the following characterization: if C is continuous and integrable (over the first argument), then C is a covariance function if and only if the function $C_\omega : \mathbb{R} \rightarrow \mathbb{R}$, defined by

$$C_\omega(u) = \int_{\mathbb{R}^d} e^{i\mathbf{h}^\top \omega} C(\mathbf{h}, u) d\mathbf{h}, \quad u \in \mathbb{R}, \quad (1)$$

is a covariance function for almost every $\omega \in \mathbb{R}^d$. Here, i is the unit imaginary number and \top is the transpose operator. This characterization has been the crux of many important results in spatiotemporal covariance modeling. Examples include the Gneiting class (Gneiting, 2002), Schlather's generalized class (Schlather, 2010), component-wise anisotropic covariances (Porcu et al., 2006), multivariate geostatistical modeling (Apanasovich & Genton, 2010), quasi-arithmetic construction (Porcu et al., 2010) and nonstationary models (Porcu et al., 2007).

Criterion (1) proves the validity of the Gneiting class of covariance functions:

$$C(\mathbf{h}; u) = \frac{\sigma^2}{\psi(u^2)^{d/2}} \varphi\left(\frac{\|\mathbf{h}\|^2}{\psi(u^2)}\right), \quad \mathbf{h} \in \mathbb{R}^d, u \in \mathbb{R}, \quad (2)$$

where $\|\cdot\|$ is the Euclidean norm. The function $\varphi : [0, \infty) \rightarrow \mathbb{R}_+$ is completely monotonic; that is, φ is infinitely differentiable on $(0, \infty)$, satisfying $(-1)^n \varphi^{(n)}(t) \geq 0$, $n \in \mathbb{N}$. Here, $\varphi^{(n)}$ denotes n th derivative and we use $\varphi^{(0)}$ for φ , and ψ is strictly positive with a completely monotonic derivative. It is also required that $\varphi(0)$ is finite.

Our paper focuses on two aspects of covariance modeling on d -dimensional spheres cross time. We first focus on Criterion (1) and its analogue on spheres over time. Our result provides an additional equivalence that completely characterizes covariance functions on spheres cross time. Then, we prove that the Gneiting class in Equation (2) can be used on d -dimensional spheres cross time where the squared Euclidean norm is replaced by the corresponding metric on the sphere. Porcu et al. (2016) considered a variant of this problem, modifying the Gneiting class based on

temporal rescaling of the spatial component. In addition to a new Gneiting class for spheres over time, we adapt Heine’s class of covariance functions (Heine, 1955), originally proposed over two-dimensional Euclidean spaces, to d -dimensional spheres cross time.

For estimation and prediction with the new covariance classes, we take a Bayesian approach using nearest-neighbor Gaussian processes (Datta et al., 2016a,b,c). Bayesian models allow for simple and rigorous uncertainty quantification through a single probabilistic framework that does not rely on asymptotic assumptions. Because Gaussian process models for large datasets, as we have with globally sampled spatiotemporal data, are often computationally intractable, we use the nearest-neighbor Gaussian process as a surrogate. Modeling with the nearest-neighbor Gaussian process enables scalable model fitting, inference, and prediction for real-data examples. Our discussion here adds to application areas for the nearest-neighbor Gaussian process as they have not been used for global data in the literature.

We start by giving background (Section 2) for the theoretical results given in Section 3. In Section 3, we generalize the Gneiting characterization of covariance functions to spheres cross time. In addition, we provide specific classes for spheres cross time. Proofs of the theoretical results are technical and are deferred to the Appendix. Appendix 4 contains a supplementary result related to our main result in Section 3. We then turn our attention to modeling data using covariance functions from our proposed classes in Section 4. In Section 5, we draw upon our modeling discussion giving data examples where our proposed covariance classes outperform covariance models currently in the literature. We provide concluding remarks in Section 6.

2 Background

The paper considers Gaussian random fields on d -dimensional spheres \mathbb{S}^d cross time (in \mathbb{R}), where \mathbb{S}^d is defined to be $\{\mathbf{s} \in \mathbb{R}^{d+1} : \|\mathbf{s}\| = 1\}$. We use the unit sphere without loss of generality. These random fields are denoted $\{Y(\mathbf{s}, t), \mathbf{s} \in \mathbb{S}^d, t \in \mathbb{R}\}$. The assumption of Gaussianity implies that finite dimensional distributions are completely specified by the mean and covariance function, and we make this assumption in modeling (Section 4).

As a metric on \mathbb{S}^d , we use the great circle distance $\theta : \mathbb{S}^d \times \mathbb{S}^d \rightarrow [0, \pi]$, defined as the mapping

$$(\mathbf{s}_1, \mathbf{s}_2) \mapsto \arccos(\mathbf{s}_1^\top \mathbf{s}_2), \quad \mathbf{s}_1, \mathbf{s}_2 \in \mathbb{S}^d.$$

We then consider covariance functions based on the great circle distance and time difference,

$$\text{cov}(Y(\mathbf{s}_1, t_1), Y(\mathbf{s}_2, t_2)) = C(\theta(\mathbf{s}_1, \mathbf{s}_2), |t_1 - t_2|), \quad (\mathbf{s}_i, t_i) \in \mathbb{S}^d \times \mathbb{R}, \quad (3)$$

where we take θ as an abbreviation for $\theta(\mathbf{s}_1, \mathbf{s}_2)$. Porcu et al. (2018) refer to such covariance functions as spatially geodesically isotropic and temporally symmetric, and Berg & Porcu (2017) provide a mathematical characterization for these functions.

Covariance functions are positive definite, meaning that for any collection $\{(\mathbf{s}_k, t_k)\}_{k=1}^N \subset \mathbb{S}^d \times \mathbb{R}$ and constants $\{a_k\}_{k=1}^N$, $\sum_{k,h} a_k a_h C(\theta(\mathbf{s}_k, \mathbf{s}_h), |t_k - t_h|) \geq 0$. This property is difficult to show mathematically. It is worth noting that classes of positive definite functions on $\mathbb{S}^d \times \mathbb{R}$ are nested, meaning that positive definiteness on $\mathbb{S}^d \times \mathbb{R}$ implies positive definiteness on $\mathbb{S}^{d'} \times \mathbb{R}$ for $d' < d$, but the converse is not necessarily true.

Porcu et al. (2016) proposed the *inverted* Gneiting class and define it as

$$C(\theta; u) = \frac{\sigma^2}{\psi_{[0,\pi]}(\theta)^{1/2}} \varphi \left(\frac{u^2}{\psi_{[0,\pi]}(\theta)} \right), \quad \theta \in [0, \pi], u \in \mathbb{R}, \quad (4)$$

with φ and ψ as defined in (2), and where $\psi_{[0,\pi]}$ denotes the restriction of ψ to the interval $[0, \pi]$. A list of the functions that can be used for this construction is provided in Tables 5 and 6 in Appendix 2. In contrast to (2) which scales Euclidean distance by a function of the temporal lag, Equation (4) rescales the temporal lag by a function of the great circle distance. It might be more intuitive to rescale space with time, as was done in (2), proposing a structure like

$$C(\theta; u) = \frac{\sigma^2}{\psi(u^2)^{d/2}} \varphi \left(\frac{\theta}{\psi(u^2)} \right), \quad \theta \in [0, \pi], u \in \mathbb{R}, \quad (5)$$

where, in this case, we do not need to restrict any of the functions φ and ψ to the interval $[0, \pi]$. Showing this construction is valid is nontrivial and receives an exposition in Section 3.2.

One choice of φ , used for construction of covariance functions in Equations (2), (4), and (5), is the Matérn class $\varphi(t) = \mathcal{M}_{\alpha,\nu}(t)$, $t \geq 0$, $\alpha, \nu > 0$, defined as

$$\mathcal{M}_{\alpha,\nu}(t) = \frac{2^{1-\nu}}{\Gamma(\nu)} \left(\frac{t}{\alpha} \right)^\nu \mathcal{K}_\nu \left(\frac{t}{\alpha} \right), \quad (6)$$

where \mathcal{K}_ν is the MacDonald function (Gradshteyn & Ryzhik, 2007). The appeal of this class is the parameter ν that governs the smoothness at the origin (Stein, 1999).

3 Theoretical Results

3.1 The Generalized Gneiting Lemma on Spheres cross Time

We begin our discussion with a characterization theorem for covariance functions defined over d -dimensional spheres cross time. Let \mathcal{G}_k^λ be the k th normalized Gegenbauer polynomial of order $\lambda > 0$ (Dai & Xu, 2013). Gegenbauer polynomials form an orthonormal basis for the space of square-integrable functions $\mathcal{L}^2([0, \pi], \sin \theta^{d-1} d\theta)$.

Theorem 1. *Let d be a positive integer. Let $C : [0, \pi] \times \mathbb{R} \rightarrow \mathbb{R}$ be continuous and bounded with the k th related Gegenbauer transform, defined as*

$$b_{k,d}(u) = \int_0^\pi C(\theta, u) \mathcal{G}_k^{(d-1)/2}(\cos \theta) \sin \theta^{d-1} d\theta, \quad u \in \mathbb{R}, k = 0, 1, \dots \quad (7)$$

with $b_{k,d} : \mathbb{R} \rightarrow \mathbb{R}$, satisfying $\sum_{k=0}^\infty \int_{\mathbb{R}} |b_{k,d}(u)| du < \infty$. Then, the following assertions are equivalent:

1. $C(\theta, u)$ is the covariance function of a random field on $\mathbb{S}^d \times \mathbb{R}$;
2. The function $C_\tau : [0, \pi] \rightarrow \mathbb{R}$, defined as

$$C_\tau(\theta) = \int_{-\infty}^{+\infty} e^{-iu\tau} C(\theta, u) du \quad (8)$$

is the covariance function of a random field on \mathbb{S}^d for almost every $\tau \in \mathbb{R}$;

3. For all $k = 0, 1, 2, \dots$, the functions $b_{k,d} : \mathbb{R} \rightarrow \mathbb{R}$, defined through (7) are continuous, positive definite on \mathbb{R} , and $\sum_k b_{k,d}(0) < \infty$.

Some comments are in order. Equivalence of 1 and 3 was shown by Berg & Porcu (2017). The result completes the picture that had been started by Gneiting (2013), Berg & Porcu (2017) and Porcu et al. (2016). Equivalence of 1 and 2 provides the analogue of Gneiting's criterion in (2) for spheres cross time. Equivalence of 2 and 3 is most surprising and could be used to find new classes of covariance functions on d -dimensional spheres cross time. Thus, Theorem 1 gives insight into relationships between covariance functions on spheres and covariance functions on Euclidean spaces. In fact, application of Theorem 1 provides a useful criterion (see Appendix 4) relating spatiotemporal covariances on $\mathbb{R} \times \mathbb{R}$ with covariance functions on $\mathbb{S}^3 \times \mathbb{R}$.

Berg & Porcu (2017) show that the restriction $\sum_{k=0}^{\infty} |\int b_{k,d}(u)| du < \infty$ is not necessary to prove the equivalence of 1 and 3, as we assume. However, this condition is not very restrictive. For illustration, take the spatiotemporal multiquadric class proposed by Porcu et al. (2016):

$$C(\theta, u) = \left(\frac{1 - \delta}{1 - \delta \rho(u) \cos \theta} \right)^{\tau}, \quad (\theta, u) \in [0, \pi] \times \mathbb{R},$$

where $\delta \in (0, 1)$ and $\tau > 0$. Here, $\rho : \mathbb{R} \rightarrow [-1, 1]$ is positive definite. Arguments in Porcu et al. (2016) show that this covariance has an absolutely convergent expansion of the type

$$C(\theta, u) = \sum_{k=0}^{\infty} \binom{\tau + k - 1}{k} \rho(u)^k \cos \theta^k, \quad (\theta, u) \in [0, \pi] \times \mathbb{R},$$

that is used to show that to satisfy the condition in Theorem 1, $u \mapsto (1 - a |\rho(u)|)^{-\tau}$ must be absolutely integrable on \mathbb{R} . This condition is easy to verify for a variety of ρ . For instance, direct inspection shows that for $\rho(u) = (1 - |u|)_+$, where $(x)_+$ denotes the truncation of x to positive values, the constraint $\tau < 1$ satisfies the necessary condition. Other examples can be obtained using, for instance, Table 1 in the Online Supplement of Porcu et al. (2016).

The proof of Theorem 1 is technical, and we defer it to Appendix 3 to avoid mathematical obfuscation.

3.2 New Classes of Covariance Functions on Spheres cross Time

We now detail our findings with two new classes of covariance functions on spheres over time.

Theorem 2. *Let d be a positive integer. Let $C : [0, \pi] \times \mathbb{R}$ be the mapping defined through Equation (5), where φ is completely monotonic on the positive real line, with $\varphi(0) < \infty$, and ψ is strictly positive with a completely monotone derivative. Then, C is a covariance function on $\mathbb{S}^d \times \mathbb{R}$.*

Again, the proof is deferred to Appendix 3. This result completes the adaptation of the Gneiting class (Gneiting, 2002) to spheres cross time. Any function φ from Table 5 in Appendix 2 can be used for the purposes of Theorem 2. Remarkably, arguments in Gneiting (2013) show that the Matérn covariance function in Equation (6) can only be used in Theorem 2 for $0 < \nu \leq 1/2$. If one is interested in smoother realizations over spheres, then a common method involves replacing the great circle distance in Equation (5) with the Euclidean distance on spheres, also

called chordal distance (Gneiting, 2013; Porcu et al., 2018). In this case, any choice for $\nu > 0$ preserves positive definiteness. At the same time, using chordal distance has a collection of drawbacks that have inspired constructive criticism in Banerjee (2005), Gneiting (2013), Porcu et al. (2018) and Alegria & Porcu (2017), to cite a few. We explore both possibilities and compare them in terms of predictive performance in Section 5.

We now introduce another class of covariance functions. We define the complementary error function erfc as

$$\text{erfc}(t) = \frac{2}{\sqrt{\pi}} \int_t^\infty \exp(-\xi^2) d\xi, \quad t \geq 0,$$

and $\text{erfc}(t) = 2 - \text{erfc}(-t)$ when t is negative. We can show the following result.

Theorem 3. *Let $\psi_{[0,\pi]}$ be the restriction to $[0, \pi]$ of a positive function with a completely monotonic derivative. Then,*

$$C(\theta, u) = e^{-|t|} \text{erfc} \left(\sqrt{\psi_{[0,\pi]}(\theta)} - \frac{|t|}{2\sqrt{\psi_{[0,\pi]}(\theta)}} \right) + e^{|t|} \text{erfc} \left(\sqrt{\psi_{[0,\pi]}(\theta)} + \frac{|t|}{2\sqrt{\psi_{[0,\pi]}(\theta)}} \right), \quad (9)$$

$\theta \in [0, \pi], u \in \mathbb{R}$, is a covariance function on $\mathbb{S}^d \times \mathbb{R}$ for all $d = 1, 2, \dots$

The class presented in Equation (9) is related to a covariance class on $\mathbb{R} \times \mathbb{R}$ considered by Heine (1955) that was constructed using a second-order partial differential equation. Again, the proof is provided in Appendix 3.

4 Modeling Nonseparable Spatiotemporal Data

4.1 Hierarchical Process Modeling for Spatiotemporal Data

We illustrate the utility of one of our covariance classes (Theorem 2) using hierarchical nearest-neighbor Gaussian process models in a Bayesian setting. In spatial and spatiotemporal analyses, Bayesian models are often preferred for hierarchical models because they allow for simple and rigorous uncertainty quantification through a single probabilistic framework that does not rely on asymptotic assumptions (see, e.g., Gelman et al., 2014; Banerjee et al., 2014).

Spatiotemporal random effects for point-referenced data are often specified through a functional prior using a Gaussian process, a subclass of Gaussian random fields. Gaussian processes are natural choices for modeling data that vary in space and time. However, likelihood computations for hierarchical Gaussian process models require inverting a square matrix with dimension equal to size of the data, making Gaussian process models intractable in “big-data” settings. Many have addressed this computational bottleneck using either low-rank or sparse matrix methods (see Heaton et al., 2017, for a review and comparison of some of these methods).

Low-rank methods depend on selecting representative points, often called knots, that are used to approximate the original process (see, e.g., Higdon, 2002; Banerjee et al., 2008; Cressie & Johannesson, 2008; Stein, 2008). These models tend to oversmooth and often have poor predictive performance (see Stein, 2014; Heaton et al., 2017).

In contrast to low-rank methods, sparsity in either the covariance matrix or the precision matrix can reduce the computational burden by inducing. Covariance tapering creates sparsity in the covariance matrix by using compactly supported covariance functions (see, e.g., Furrer et al., 2006;

Kaufman et al., 2008; Furrer et al., 2012). These methods are generally effective for parameter estimation and interpolation; however, the allowable class of covariance functions is limited. On the other hand, inducing sparsity in the precision matrix has been leveraged to approximate Gaussian processes using Markov random fields (Rue et al., 2009) or using conditional likelihoods (Vecchia, 1988; Stein et al., 2004). These approaches were extended to process modeling by Gramacy & Apley (2015) and Datta et al. (2016a). Unlike local approximate Gaussian processes (Gramacy & Apley, 2015), the nearest-neighbor Gaussian process is itself a Gaussian process (Datta et al., 2016a) and has good predictive performance relative to other “fast” Gaussian process methods (See Heaton et al., 2017).

To specify a nearest-neighbor Gaussian process, we begin with a parent Gaussian process over $\mathbb{R}^d \times \mathbb{R}$ or $\mathbb{S}^d \times \mathbb{R}$. Nearest-neighbor Gaussian process models induce sparsity in the precision matrix of the parent Gaussian model by assuming conditional independence given neighborhood sets (Datta et al., 2016a,b,c). This assumption induces a Gaussian directed acyclic graph and has huge computational benefits (see Datta et al., 2016a, for discussion). Modeling, model fitting, and prediction details for nearest-neighbor Gaussian process models are given in Appendix 4.

4.2 Examples of Covariance Functions

Here, we turn our attention to nonseparable covariance examples used in Section 5 and in Appendix 6. We focus on six covariance models which we compare using real and simulated data. For all examples, we parameterize the models with variance σ^2 and use c_s and c_t to represent the strictly positive spatial and temporal scale parameters, respectively.

Explicitly, we consider two special cases from the Gneiting class (2) with $\varphi(t) = \mathcal{M}_{\alpha,\nu}(t)$, $t \geq 0$, for $\mathcal{M}_{\alpha,\nu}$, defined in (6), obtained when $\nu = 1/2$ and $\nu = 3/2$,

$$C(\mathbf{h}, u) = \frac{\sigma^2}{\left(1 + \left(\frac{\|\mathbf{h}\|}{c_t}\right)^\alpha\right)^{\delta+\beta d/2}} \mathcal{M}_{c_s,\nu} \left(\frac{\|\mathbf{h}\|}{\left(1 + \left(\frac{\|u\|}{c_t}\right)^\alpha\right)^{\beta/2}} \right), \quad (\mathbf{h}, u) \in \mathbb{R}^d \times \mathbb{R}. \quad (10)$$

These choices correspond to $\mathcal{M}_{1,1/2}(t) = \exp(-t)$ and $\mathcal{M}_{1,3/2}(t) = \exp(-t)(1+t)$, $t \geq 0$. Here, we work on the sphere, thus $\|\cdot\|$ refers to chordal distance. The parameters restriction is $\delta > 0$, $\beta \in (0, 1]$ and $\alpha \in (0, 2]$.

Next, we consider a pair of similar covariance models from the inverted Gneiting class (Porcu et al., 2016) in Equation (4):

$$C(\theta, u) = \frac{\sigma^2}{\left(1 + \left(\frac{\theta}{c_s}\right)^\alpha\right)^{\delta+\beta/2}} \exp \left(- \frac{|u|^{2\gamma}}{c_t^{2\gamma} \left(1 + \left(\frac{\theta}{c_s}\right)^\alpha\right)^{\beta\gamma}} \right), \quad (\theta, u) \in [0, \pi] \times \mathbb{R}, \quad (11)$$

where $\delta > 0$, and where β, α and γ belong to the interval $(0, 1]$. The second we consider uses the generalized Cauchy covariance function (Gneiting & Schlather, 2004, see Tables 5 and 6 in Appendix 2) for the temporal margin,

$$C(\theta, u) = \frac{\sigma^2}{\left(1 + \left(\frac{\theta}{c_s}\right)^\alpha\right)^{\delta+\beta/2}} \left(1 + \frac{|u|^{2\gamma}}{c_t^{2\gamma} \left(1 + \left(\frac{\theta}{c_s}\right)^\alpha\right)^{\beta\gamma}} \right)^{-\lambda}, \quad (\theta, u) \in [0, \pi] \times \mathbb{R}, \quad (12)$$

with $\delta, \lambda > 0$, and where β, α and γ belong to the interval $(0, 1]$.

From the Gneiting class on spheres (see Theorem 2), we give two examples that mirror those presented in Equations (11) and (12):

$$C(\theta, u) = \frac{\sigma^2}{\left(1 + \left(\frac{|u|}{c_t}\right)^\alpha\right)^{\delta+\beta d/2}} \exp\left(-\frac{\theta^\gamma}{c_s^\gamma \left(1 + \left(\frac{|u|}{c_t}\right)^\alpha\right)^{\beta\gamma}}\right), \quad (\theta, u) \in [0, \pi] \times \mathbb{R}, \quad (13)$$

with $\delta > 0$, $\beta, \gamma \in (0, 1]$ and $\alpha \in (0, 2]$. For the second, we propose again a generalized Cauchy covariance function for the spatial margin, obtaining

$$C(\theta, u) = \frac{\sigma^2}{\left(1 + \left(\frac{|u|}{c_t}\right)^\alpha\right)^{\delta+\beta d/2}} \left(1 + \frac{\theta^\gamma}{c_s^\gamma \left(1 + \left(\frac{|u|}{c_t}\right)^\alpha\right)^{\beta\gamma}}\right)^{-\lambda}, \quad (\theta, u) \in [0, \pi] \times \mathbb{R}, \quad (14)$$

where $\delta > 0$, $\beta, \gamma \in (0, 1]$, $\alpha \in (0, 2]$ and $\lambda > 0$.

For all models in both real data analysis and simulation, the variance σ^2 is augmented with a nugget effect (denoted τ^2 throughout) to account for potential discontinuities at the origin of the covariance function.

We provide a brief simulation study in Appendix 6 to demonstrate that covariance model parameters could be estimated reasonably well using a nearest-neighbor Gaussian process model. Additionally, we show that predictive performance of the generative model is as good or better than competing models. To illustrate practical advantages of the new Gneiting class using spherical distance (Theorem 2), we carry out analyses on two climate reanalysis datasets from the National Centers for Environmental Prediction and National Center for Atmospheric Research climate (Kalnay et al., 1996). For both analyses, we use the first week of the 2017 dataset.

4.3 Model Comparison

To compare models that differ in terms of covariance specification, we propose the following criteria: $100 \times \alpha$ % predictive interval coverage, predictive mean square or absolute error (defined as $(\mathbf{E}(Y_i | \mathbf{Y}_{obs}) - y_i)^2$ or $|\mathbf{E}(Y_i | \mathbf{Y}_{obs}) - y_i|$, respectively), where \mathbf{Y}_{obs} denotes observations. We also use the continuous ranked probability score (CRPS), where

$$\text{CRPS}(F_i, y_i) = \int_{-\infty}^{\infty} (F_i(x) - \mathbf{1}(x \geq y_i))^2 dx = \mathbf{E} | Y_i - y_i | - \frac{1}{2} \mathbf{E} | Y_i - Y'_i |, \quad (15)$$

and F_i denotes the predictive distribution for Y_i (Gneiting & Raftery, 2007). An empirical estimate of the continuous ranked probability score, using M posterior predictive samples of $Y_i | \mathbf{Y}_{obs}$, is

$$\text{CRPS}(\hat{F}_i, y_i) = \frac{1}{M} \sum_{j=1}^M | Y_j - y_i | - \frac{1}{2M^2} \sum_{j=1}^M \sum_{k=1}^M | Y_j - Y_k |. \quad (16)$$

We average continuous ranked probability scores over all held-out data to obtain a single value for comparison.

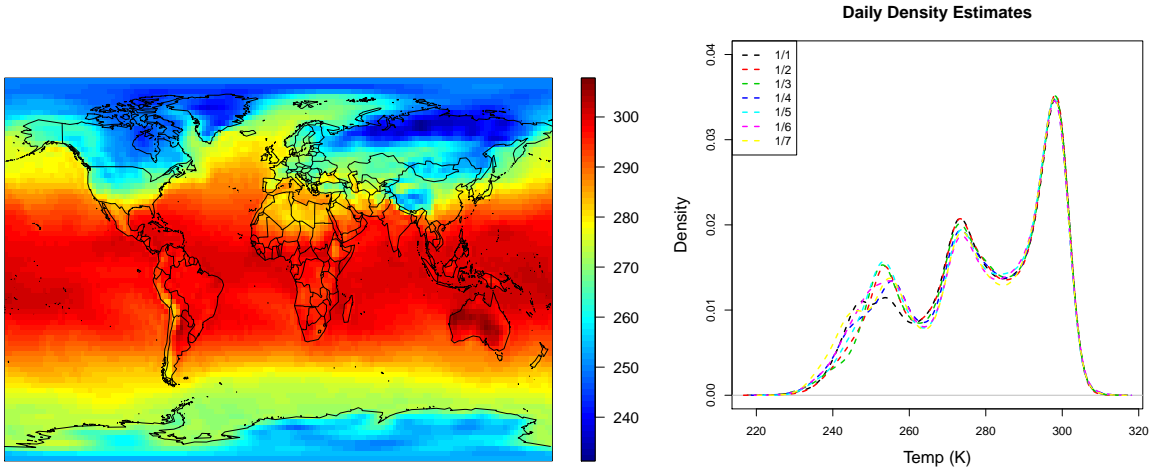
5 Data Examples

5.1 Surface Air Temperature Reanalysis Data

For this section, we utilize the 2017 National Centers for Environmental Prediction/National Center for Atmospheric Research daily average 0.995 sigma level (near-surface) temperature reanalysis data (Kalnay et al., 1996). Air temperature at 0.995 sigma level is defined to be the temperature taken at an air pressure $0.995 \times$ surface air pressure.

The foundations of global temperature change are well established (see, e.g., Folland et al., 2001; Hansen et al., 2006, 2010). Furthermore, air temperature changes have, along with other changes in climate, a wide and deep impact on global water and biological systems (see Parmesan & Yohe, 2003; Thomas et al., 2004; Held & Soden, 2006). For these reasons, many climate models are dedicated to understanding past and predicting future temperature changes (see Simmons et al., 2004, for some discussion and comparisons about the various analyses of surface air temperature).

The daily near-surface temperature reanalysis data gives daily temperature averages over a global grid with 2.5° spacing for latitude and longitude. We thin the data to 5° spacing for latitude and longitude to carry out model comparison on the held-out data. In this dataset, we have observations at 2522 unique spatial locations, giving 17654 total observations. The spatial averages of near-surface temperature over the first week of January are plotted in Figure 1a. Additionally, we give the density estimate of near-surface temperature for each day in Figure 1b. Figure 1b shows that the overall temperature distribution is similar across days, and Figure 1a demonstrates a clear spatial structure. Because our covariance model allows space to be scaled by time while using the spherical distance, we expect that our model may be able to capture the strong spatial structure in this data more effectively than the models with which we compare them.



(a) Near-surface temperature heat map in degrees Kelvin (K). (b) Kernel density estimates of global near-surface temperature for each day.

With 17654 data, carrying out fully Bayesian inference using a full Gaussian process model is computationally burdensome; thus, we utilize a nearest-neighbor Gaussian process model. For these models, we use simple neighborhood selection presented in Datta et al. (2016c) using $m = 25$

neighbors, using the five nearest-neighbors at the five most recent times, including the current time. We utilize two covariance models from each of the Gneiting class, the inverted-Gneiting class using spherical distance, and our new Gneiting class (Theorem 2). These models are presented in Equations (10) to (14). For all models, we use inverse-gamma prior distributions for τ^2 and σ^2 with 0.1 for both the shape and rate parameters. We use prior distributions of $c_s \sim \text{Unif}(0, \pi)$, $c_t \sim \text{Unif}(0, 10)$, $\alpha \sim \text{Unif}(0, 2]$, and $\beta \sim \text{Unif}(0, 1]$ for correlation function parameters. Because many covariance models have limited parameter identifiability (see Zhang, 2004, for discussion of the Matérn class), we constrain $\delta + \beta d/2 = 1$ for Equations (10), (13), (14), and $\delta + \beta/2 = 1$ for Equations (11) and (12).

We compare these six models in terms of predictive performance on a randomly selected subset of the held-out data. In total, we use 1000 locations over the week, giving 7000 hold-out observations. These hold-out locations are plotted in Figure 5 in Appendix 7. We compare these models in terms of predictive root mean squared error, mean absolute error, continuous ranked probability score, and 90% prediction interval coverage, as discussed in Section 4.3. For predictions, neighbors are chosen to make prospective predictions using 25 neighbors (See Appendix 5).

The results presented are based on 25,000 posterior draws after a burn-in of 5,000 iterations using a Gibbs sampler presented in Appendix 5. These posterior samples are used for prediction and posterior inference. The results of the model comparison are given in Table 1. For this data, the covariance models from our class Equations (13) and (14) had the best out-of-sample predictive performance, and the model (14) was best. For comparison, the Gneiting classes using chordal distance (Equation (10)) had continuous ranked probability scores 4% and 14% higher than the best model for $\nu = 1/2$ and $\nu = 3/2$, respectively. Both models from the inverted Gneiting class with spherical distance were 10% worse in terms of continuous ranked probability scores.

Equation	PRMSE	PMAE	90% Coverage	CRPS	Relative CRPS
(10) and $\nu = 1/2$	6.44	4.58	0.91	3.50	1.04
(10) and $\nu = 3/2$	7.15	5.08	0.91	3.81	1.14
(11)	6.79	4.85	0.90	3.70	1.10
(12)	6.78	4.84	0.90	3.69	1.10
(13)	6.08	4.44	0.90	3.38	1.01
(14)	6.04	4.40	0.90	3.35	1.00

Table 1: Predictive performance of competing covariance models for the cloud cover dataset. For brevity in the table, let PRMSE and PMAE denote predictive mean squared error and mean absolute error, respectively. Relative CRPS is scaled such that the lowest is one. Bolded entries are used to indicate best model performances (i.e. lowest PRMSE, PMAE, and CRPS and 90% interval coverage closest to 90%).

For the best model, Equation (14), we provide posterior summaries in Table 2. Additionally, we display the correlation contour as function of spherical distance θ and time t for the posterior mean in Figure 2.

	Mean	Standard Deviation	2.5%	97.5%
τ^2	23.229	0.476	22.308	24.176
σ^2	126.590	3.399	119.973	133.386
c_s	6.253	0.030	6.173	6.282
c_t	9.754	0.234	9.100	9.994
α	1.999	5.4e-4	1.998	2.000
β	0.978	0.022	0.921	0.999

Table 2: Posterior summaries for the near-surface air temperature datasets for parameters for the model fit using Equation (13). Percentiles (2.5% and 97.5%) represent posterior percentiles.

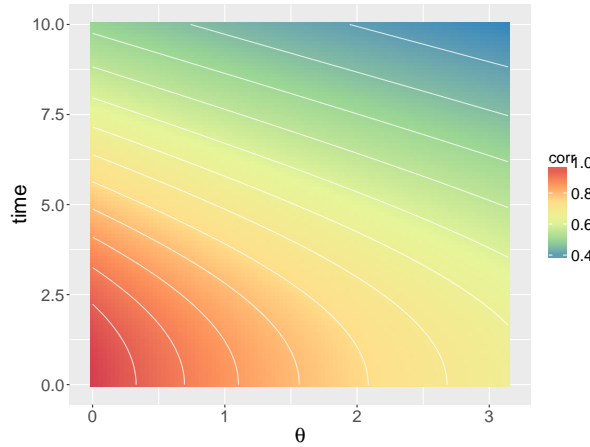


Figure 2: Posterior mean correlation contour plot for the near-surface air temperature.

We can interpret $\sigma^2/(\sigma^2 + \tau^2)$ as the proportion of total variance attributable to the spatiotemporal random effect. In other words, our selected covariance model accounts for 84.39% of the total variance (see Table 2). In Table 2, c_s and c_t suggest that the surface temperature process exhibits persistent correlation over both space and time, and high values of α , close to two, suggest that the temperature process is very smooth. Lastly, and importantly, the separability parameter $\beta \in [0, 1]$ is near one, meaning that the space-time process is highly nonseparable.

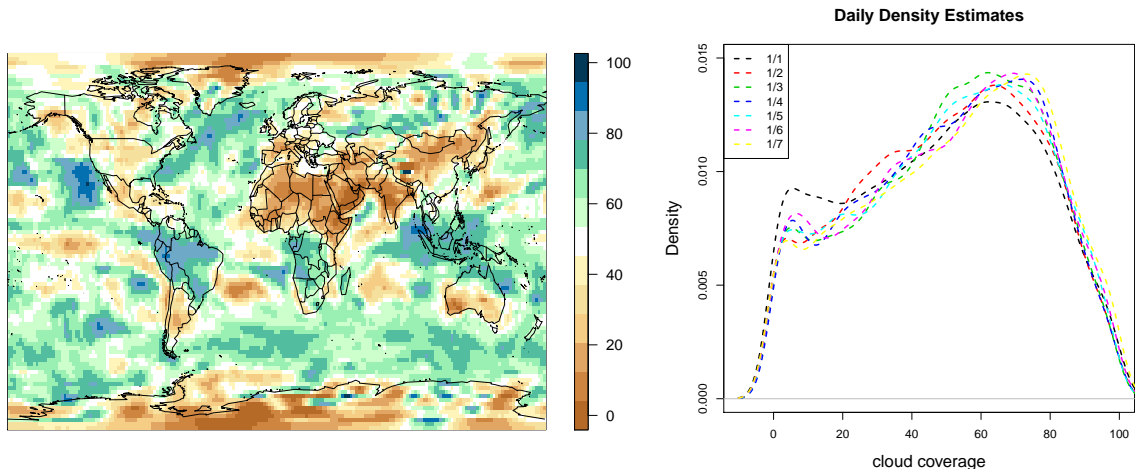
5.2 Total Cloud Coverage Reanalysis Data

For this section, we utilize the 2017 National Centers for Environmental Prediction/National Center for Atmospheric Research daily average total cloud coverage reanalysis data (Kalnay et al., 1996). Total cloud coverage is defined as the fraction of the sky covered by any visible clouds, regardless of type. Total cloud coverage takes values between 0 and 100, representing a percentage of cloud coverage. Values of total cloud coverage close to 0 indicate clear skies, values from 40 to 70 percent represent broken cloud cover, and overcast skies correspond with 70 to 100 percent.

The degree of cloudiness impacts how much solar energy radiates to the Earth (see, e.g., Svensmark & Friis-Christensen, 1997). Total cloud coverage, like changes in global surface temperature, has been impacted by global climate changes (see, e.g., Melillo et al., 1993; Wylie et al., 2005), and changes in total cloud coverage are linked with many biological changes (see Pounds et al., 1999).

Thus, tracking, predicting, and anticipating changes in cloudiness have important implications for understanding global climate changes and their effects on ecosystems.

The daily total cloud coverage reanalysis data represent daily averages and are given on a global grid with 1.9° spacing for latitude and 1.875° spacing for longitude. The spatial averages of cloud coverage over the first week of January are plotted in Figure 3a. This map shows clear spatial variability that suggests that a spatial model is appropriate. We provide density estimates of total cloud coverage for each day of the week in Figure 3b. As we did with temperature, we see from Figure 3b that cloud coverage appears similar across days.



(a) Total cloud coverage heat map in percentage, taking values 0 to 100. (b) Kernel density estimates of total cloud coverage for each day.

Again, we thin the data to 3.8° spacing for latitude and 3.75° for longitude to carry out model comparison on held-out data. In total, we have 4512 unique spatial locations, giving 31584 total observations. With 31584 data, carrying out fully Bayesian inference using a full Gaussian process model is intractable; thus, we utilize a nearest-neighbor Gaussian process model. For these models, we use the same neighborhood formulations and fit the same covariance models with the same prior distribution to these data as we did in Section 5.1.

To obtain a test set to compare the six competing models, we randomly select 1000 locations and predict at these locations over the time-span of our data, giving a test set of size 7000. These hold-out locations are plotted in Figure 6 in Appendix 7. As before, we compare these models in terms of predictive mean squared error, mean absolute error, continuous ranked probability scores, and 90% prediction interval coverage, as discussed in Section 4.3. The results of the model comparison are given in Table 3.

Equation	PRMSE	PMAE	90% Coverage	CRPS	Relative CRPS
(10) and $\nu = 1/2$	13.92	11.08	0.95	7.85	1.32
(10) and $\nu = 3/2$	13.35	10.51	0.94	7.53	1.26
(11)	19.89	8.27	0.90	8.27	1.39
(12)	19.31	8.18	0.90	8.15	1.37
(13)	21.68	16.86	0.88	11.74	1.97
(14)	10.68	7.66	0.95	5.96	1.00

Table 3: Predictive performance of competing covariance models for the total cloud coverage dataset. For brevity in the table, let PRMSE and PMAE denote predictive mean squared error and mean absolute error, respectively. Relative CRPS is scaled such that the lowest is one. Bolded entries are used to indicate best model performance (i.e. lowest PRMSE, PMAE, and CRPS and 90% interval coverage closest to 90%).

Interestingly, our new class had the best and worst models in terms of prediction for the total cloud coverage dataset. All competing models were at least 26% worse in terms of continuous ranked probability score compared to the best model (14).

For the best predictive model in Equation (14), we provide posterior summaries in Table 4. Additionally, we display the correlation contour as function of spherical distance θ and time t for the posterior mean in Figure 4. The scale of the plots in Figure 4 are not the same as Figure 2. Correlation falls off sharply as a function of great circle distance. In this way, the total cloud coverage dataset differs greatly from the near-surface temperature dataset which demonstrated very persistent autocorrelation over space and time.

	Mean	Std. Err.	2.5%	97.5%
τ^2	22.280	3.601	16.764	31.598
σ^2	595.93	7.677	580.318	610.792
c_s	0.102	0.004	0.094	0.110
c_t	6.762	1.794	3.416	9.803
α	0.350	0.071	0.232	0.516
β	0.952	0.049	0.817	0.999

Table 4: Posterior summaries for the total cloud coverage datasets for parameters for the model fit using Equation (13). Percentiles (2.5% and 97.5%) represent posterior percentiles.

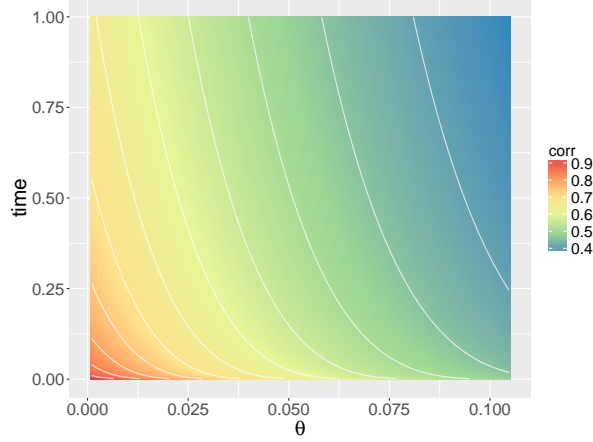


Figure 4: Posterior mean correlation contour plot for total cloud coverage data. (Left) Contour Plot (Right) Heat Map.

For the total cloud coverage data, spatiotemporal variance σ^2 accounts for 96.40% of the total variance $\sigma^2 + \tau^2$ (see Table 4). In Table 4, the parameter c_t suggests that the surface temperature process exhibits persistent correlation over time; however, as discussed, the parameter c_s indicates rapid decay as a function of space. Unlike the temperature data, the smoothness parameter α takes low values, suggesting less smoothness in the total cloud coverage process. The separability parameter $\beta \in [0, 1]$ was again close to one, meaning that the covariance process is nonseparable.

6 Discussion and Conclusion

In this paper, we generalize the Gneiting criteria for nonseparable covariance functions (Gneiting, 2002) in Theorem 1 and present new classes of nonseparable covariance models for spatiotemporally evolving data in Theorems 2 and 3. Beyond simply generalizing the Gneiting criteria, this theorem gives an avenue for discovering new nonseparable covariance classes. We then illustrate the utility of our new Gneiting class using spherical distance through a simulation study and two climate reanalysis datasets from the National Centers for Environmental Prediction and National Center for Atmospheric Research (Kalnay et al., 1996). In the simulation study, we demonstrated that we could estimate model parameters reasonably well and showed that predictive performance of the generative model is as good or better than competing models. We then give two data examples where covariance models from our class outperform analogous nonseparable covariance models from Gneiting (2002) and Porcu et al. (2016). These results highlight the benefit of allowing spatial distance to be scaled by the difference in time and the importance of using the spherical distance relative to Euclidean distance or chordal distance.

The result in Theorem 1 presents a key for extending results obtained in Euclidean spaces to spheres cross time. Due to the lack of literature for multivariate cross-covariance models on spheres over time, with the notable exception of Alegria et al. (2017), we recommend this as a valuable area of expansion. In addition, development of nonstationary covariance models for spheres cross time is an important direction for future research.

Appendix 1

Mathematical Background

To allow for neat exposition, some background material is necessary. We define Φ_d (Schoenberg, 1938) as the class of continuous functions $f : [0, \infty) \rightarrow \mathbb{R}$, with $f(0) < \infty$, such that $f(\|\cdot\|^2)$ is positive definite on \mathbb{R}^d . Accordingly, we define $\Phi_\infty = \bigcap_{d \geq 1} \Phi_d$ as the class of continuous functions $f : [0, \infty) \rightarrow \mathbb{R}$ such that $f(\|\cdot\|^2)$ is positive definite on any d -dimensional Euclidean space.

We follow Porcu et al. (2006) when defining the class $\Phi_{d,T}$ of continuous functions $f : [0, \infty)^2 \rightarrow \mathbb{R}$ such that $f(0, 0) < \infty$ and such that the function $f(\|\cdot\|^2, |\cdot|)$ is positive definite on $\mathbb{R}^d \times \mathbb{R}$. Accordingly, we call $\Phi_{\infty,T} = \bigcap_{d \geq 1} \Phi_{d,T}$ the class of continuous functions f such that $f(\|\cdot\|^2, |\cdot|)$ is positive definite on any d -dimensional Euclidean space. According to Porcu et al. (2006), $f \in \Phi_{\infty,T}$ if and only if

$$f(x, t) = \int_{[0, \infty)} \int_{[0, \infty)} e^{-x\xi_1} \cos(t\xi_2) F(d(\xi_1, \xi_2)), \quad x, t \in [0, \infty), \quad (17)$$

where F is a positive and bounded measure. Arguments in theorem 1 of Gneiting (2002) show that the function

$$f(x, t) = \frac{1}{\psi(t)} \varphi\left(\frac{x}{\psi(t)}\right), \quad x, t \in [0, \infty), \quad (18)$$

for φ being completely monotonic and ψ a positive function with completely monotonic derivative, belongs to the class $\Phi_{\infty,T}$.

We follow Gneiting (2013) to define Ψ_d as the class of continuous functions $g : [0, \pi] \rightarrow \mathbb{R}$ with $g(0) < \infty$ and such that $g(\theta)$ is positive definite on \mathbb{S}^d , for θ being the great circle distance. Let us define $\Psi_{d,T}$ (Berg & Porcu, 2017) as the class of continuous functions $g : [0, \pi] \times \mathbb{R} \rightarrow \mathbb{R}$ with $g(0, 0) < \infty$, such that $g(\theta, |u|)$ is positive definite on $\mathbb{S}^d \times \mathbb{R}$. Analogously, we define $\Psi_{\infty,T}$ as $\bigcap_{d \geq 1} \Psi_{d,T}$ and $\Psi_\infty = \bigcap_{d \geq 1} \Psi_d$. In the following, we write $L_1(\mathbb{R})$ for the space of absolutely integrable functions on \mathbb{R} .

Appendix 2

Useful Functions for Construction of Covariance Functions According to Theorem 2

Here, we provide tables of functions that are useful for constructing the covariance models provided in this paper. We denote $\varphi(\cdot)$ as any completely monotonic function being finite at zero, and we let $\psi(\cdot)$ be functions that are strictly positive and have a completely monotonic derivative. Examples of *phi* and *psi* are given in Tables 5 and 6, respectively.

Families for φ	Expression	Parameters
Dagum	$\varphi(t) = 1 - \left(\frac{t^\beta}{1+t^\beta}\right)^\tau$	$\beta, \tau \in (0, 1]$
Matérn	Equation (6)	$0 < \nu \leq 1/2$
Gen. Cauchy	$\varphi(t) = (1 + t^\alpha)^{-\beta/\alpha}$	$\alpha \in (0, 1], \beta > 0$
Pow. Exponential	$\varphi(t) = \exp(-t^\alpha)$	$\alpha \in (0, 1]$

Table 5: Examples of completely monotonic functions.

Families for ψ	Expression	Parameters
Dagum	$\psi(t) = 1 + \left(\frac{t^\beta}{1+t^\beta}\right)^\tau$	$\beta, \tau \in (0, 1]$
Gen. Cauchy	$\psi(t) = (1 + t^\alpha)^{\beta/\alpha}$	$\alpha \in (0, 1], \beta \leq \alpha$
Power	$\psi(t) = c + t^\alpha$	$\alpha \in (0, 1], c > 0$

Table 6: Examples of functions that are strictly positive and have a completely monotonic derivative.

Appendix 3

Proof of Theorem 1

We start by proving the implication (1) \longrightarrow (2). Let $C \in \Psi_{d,T}$. Then, according to Theorem 3.3 in Berg & Porcu (2017), C admits the expansion

$$C(\theta, u) = \sum_{k=0}^{\infty} b_{k,d}(u) \mathcal{G}_k^{(d-1)/2}(\cos \theta), \quad (\theta, u) \in [0, \pi] \times \mathbb{R}, \quad (19)$$

with $b_{k,d}$ being positive definite on \mathbb{R} for all $k = 0, 1, \dots$, and with $\sum_{k=0}^{\infty} b_{k,d}(0) < \infty$. Let us start by noting that the assumption $\sum_k \int |b_{k,d}(u)| du < \infty$ implies $C(\theta, \cdot) \in L_1(\mathbb{R})$ for all $\theta \in [0, \pi]$.

In fact,

$$\begin{aligned} \int_{-\infty}^{\infty} |C(\theta, u)| du &= \int_{-\infty}^{\infty} \left| \sum_{k=0}^{\infty} b_{k,d}(u) \mathcal{G}_k^{(d-1)/2}(\cos \theta) \right| du \\ &\leq \sum_{k=0}^{\infty} \int_{-\infty}^{\infty} |b_{k,d}(u)| du < \infty, \end{aligned}$$

where the last step is justified by the fact that, for normalized Gegenbauer polynomials, $|\mathcal{G}_k(u)| \leq \mathcal{G}_k(1)$.

Let C_τ be the function defined through (8). Since $C(\theta, \cdot) \in L_1(\mathbb{R})$ for all θ , and using Lebesgue's theorem, we have

$$\begin{aligned} C_\tau(\theta) &= \int_{-\infty}^{+\infty} e^{-iu\tau} C(\theta, u) du \\ &= \int_{-\infty}^{+\infty} e^{-iu\tau} \sum_{k=0}^{\infty} b_{k,d}(u) \mathcal{G}_k^{(d-1)/2}(\cos \theta) du \\ &= \sum_{k=0}^{\infty} \hat{b}_{k,d}(\tau) \mathcal{G}_k^{(d-1)/2}(\cos \theta), \quad \theta \in [0, \pi], \end{aligned}$$

where $\hat{b}_{k,d}(\tau) = \int_{-\infty}^{+\infty} e^{-iu\tau} b_{k,d}(u) du$. Clearly, for any $k = 0, 1, \dots$ we have that $\hat{b}_{k,d}$ is nonnegative and additionally $\hat{b}_{k,d} \in L_1(\mathbb{R})$. To complete the proof, we invoke Schoenberg (1942) Theorem and thus need to show that $\sum_k \hat{b}_{k,d}(\tau) < \infty$ for all $\tau \in \mathbb{R}$. Again invoking Lebesgue's theorem we have

$$\begin{aligned} \sum_{k=0}^{\infty} \hat{b}_{k,d}(\tau) &= \sum_{k=0}^{\infty} \int_{-\infty}^{+\infty} e^{-iu\tau} b_{k,d}(u) du \\ &= \int_{-\infty}^{+\infty} e^{-iu\tau} \sum_{k=0}^{\infty} b_{k,d}(u) du \\ &= \int_{-\infty}^{+\infty} e^{-iu\tau} B_d(u) du, \end{aligned}$$

with $B_d(u) = \sum_{k=0}^{\infty} b_{k,d}(u)$. Using the fact that $\sum_{k=0}^{\infty} b_{k,d}(0) < \infty$ and that $b_{k,d}(0) > |b_{k,d}(u)|$ for all $u \in \mathbb{R}$ (because $b_{k,d}$ are positive definite for all k), we get

$$\infty > \sum_{k=0}^{\infty} b_{k,d}(0) \geq \sum_{k=0}^{\infty} |b_{k,d}(u)| \geq \sum_{k=0}^{\infty} b_{k,d}(u) = B_d(u), \quad u \in \mathbb{R},$$

showing that B_d is bounded and continuous. Further, B_d is positive definite on \mathbb{R} because positive definite functions are a convex cone being closed under pointwise convergence. To complete the result, we need to prove that $B_d \in L_1(\mathbb{R})$. This comes from the fact that

$$\int B_d(u) du = C(0, u) \in L_1(\mathbb{R}).$$

The proof is completed.

To prove (2) \longrightarrow (1), we let C_τ as defined through (8) and suppose that $C_\tau \in \Psi_d$ a.e. $\tau \in \mathbb{R}$. By Schoenberg (1942) theorem, we have that

$$\tilde{b}_{k,d}(\tau) := \kappa \int_0^\pi C_\tau(\theta) \mathcal{G}_k^{(d-1)/2}(\cos \theta) \sin \theta^{d-1} d\theta, \quad \tau \in \mathbb{R}, \quad (20)$$

is nonnegative, where $\kappa > 0$ (Berg & Porcu, 2017). Additionally, for any $\tau \in \mathbb{R}$, we have $\sum_k \tilde{b}_{k,d}(\tau) < \infty$. Now Fourier inversion allows to write

$$\begin{aligned} C(\theta, u) &= \frac{1}{2\pi} \int_{-\infty}^{+\infty} e^{iu\tau} C_\tau(\theta) d\tau \\ &= \sum_{k=0}^{\infty} b_{k,d}(u) \mathcal{G}_k(\cos \theta), \quad \theta \in [0, \pi], u \in \mathbb{R}, \end{aligned}$$

with the last step justified by the properties of the functions $\tilde{b}_{k,d}$, and where $b_{k,d}(\cdot)$ is positive definite on \mathbb{R} for all $n \in \mathbb{N}$. Thus, the proof is completed by invoking Theorem 3.3 in Berg & Porcu (2017) and by verifying that

$$\sum_{k=0}^{\infty} b_{k,d}(0) = \sum_{k=0}^{\infty} \int_{-\infty}^{+\infty} \tilde{b}_{k,d}(\tau) d\tau < \infty.$$

We now prove the implication (2) \longrightarrow (3). Since $C_\tau \in \Psi_d$ for almost every $\tau \in \mathbb{R}$, we have that (20) holds. This implies that

$$b_{k,d}(u) = \frac{1}{\pi} \int_{-\infty}^{+\infty} e^{iu\tau} \tilde{b}_{k,d}(\tau) d\tau, \quad k = 0, 1, \dots,$$

is positive definite. Summability of the sequence $\{b_{k,d}(u)\}_{k=0}^{\infty}$ at $u = 0$ follows easily from previous arguments.

To prove the implication (3) \longrightarrow (2), using Equation (7) we have

$$\begin{aligned} b_{k,d}(u) &= \int_0^\pi C(\theta, u) \mathcal{G}_k^{(d-1)/2}(\cos \theta) \sin \theta^{d-1} d\theta \\ &= \frac{1}{2\pi} \int_{-\infty}^{+\infty} e^{iu\tau} \int_0^\pi C_\tau(\theta) \mathcal{G}_k(\theta) \sin \theta^{d-1} d\theta d\tau, \end{aligned}$$

which shows that $C_\tau \in \Psi_d$ for all τ because the positive definiteness of $b_{k,d}(\cdot)$ implies, by Lemma 4.3 in Berg & Porcu (2017), the inner integral $\int_0^\pi C_\tau(\theta) \mathcal{G}_k(\theta) \sin \theta^{d-1} d\theta$ to be nonnegative.

To conclude, the implication (3) \longrightarrow (1) has been shown by Berg & Porcu (2017) \square

Proof of Theorem 2

We prove the result by direct construction. (Gneiting, 2002, theorem 2) has shown that the function f in (18) belongs to the class $\Psi_{\infty, T}$. Thus, it admits a scale mixture representation of the type (17). Now, define $g(x, t) = f_{[0, \pi]}(x, t)$ as the restriction of f in (18) to the interval $[0, \pi]$ in the first

argument. Arguments in Lemma 7 in Gneiting (2013) show that $\theta \mapsto \exp(-\theta)$ belongs to the class Ψ_∞ . Thus, g is the scale mixture of an element of the class Ψ_∞ with the cosine function against a positive and bounded measure. Since the mapping $u \mapsto \cos(|u|)$ is positive definite on \mathbb{R} , and using the fact that the class $\Psi_{\infty,T}$ is a convex cone, being closed under scale mixture, we complete the proof. \square

Proof of Theorem 3

We make use of the arguments in the proof of Theorem 2, in concert with formula (15) on page 15 of Bateman (1954):

$$\frac{\pi}{2} \int_0^\infty \cos(t\omega) \exp(-(1+\omega^2)x) \frac{d\omega}{1+\omega^2} = e^{-u} \operatorname{erfc}\left(\sqrt{x} - \frac{t}{2\sqrt{x}}\right) + e^u \operatorname{erfc}\left(\sqrt{x} + \frac{t}{2\sqrt{x}}\right),$$

for $x, t \geq 0$. We now replace x with $\psi_{[0,\pi]}(\theta)$ and t with $|u|$. Since the composition of the negative exponential with a positive functions having completely monotonic derivative provides a completely monotonic function, we can invoke again Lemma 7 in Gneiting (2013) to infer that the mixture above provides, in view of analogous arguments to the proof of Theorem 2, an element of the class $\Psi_{\infty,T}$. The proof is completed. \square

Appendix 4

Supplementary Theorem for Section 3.1

We now show how Theorem 1 can be useful to understand connections and analogies between the class $\Phi_{1,T}$ and the class $\Psi_{1,T}$.

Theorem 4. *Let $\varphi : \mathbb{R} \times \mathbb{R} \rightarrow \mathbb{R}$ be a covariance function that is symmetric in both arguments. Let $\varphi_\tau : \mathbb{R} \rightarrow \mathbb{R}$ be the function defined by*

$$\varphi_\tau(x) = \int_{-\infty}^{+\infty} e^{i u \tau} \varphi(x, u) du, x \in \mathbb{R}. \quad (21)$$

and suppose that such an integral is well defined. Let $\varphi_\tau(x) = 0$ whenever $|x| \geq \pi$. Call $C(\theta, u) = \varphi_{[0,\pi]}(\theta, u)$, $\theta \in [0, \pi]$, $u \in \mathbb{R}$, where the restriction to $[0, \pi]$ is with respect to the first argument. Then, $C(\theta, u)$ is a covariance function on $\mathbb{S}^3 \times \mathbb{R}$.

Proof. Since $C \in \Phi_{1,T}$, Theorem 1 shows that φ_τ is positive definite on \mathbb{R} almost every $\tau \in \mathbb{R}$. Additionally, $\varphi_\tau(x) = 0$ for $|x| \geq \pi$. Thus, Corollary 3 in Gneiting (2013) shows that the coefficients $\hat{b}_{k,1}(\tau)$, $\tau \in \mathbb{R}$, as defined in Equation (20) are nonnegative and strictly decreasing in k for any fixed $\tau \in \mathbb{R}$. This implies that $\varphi_\tau \in \Psi_3$ for almost every $\tau \in \mathbb{R}$. Application of Theorem 1, Assertion 2, shows that $C(\theta, u) \in \Psi_{3,T}$. The proof is completed. \square

Appendix 5

Modeling Details for the Nearest-Neighbor Gaussian Process

Suppose we begin with a parent Gaussian process over $\mathbb{R}^d \times \mathbb{R}$ or $\mathbb{S}^d \times \mathbb{R}$. Nearest-neighbor Gaussian processes induce sparsity in the precision matrix of the parent Gaussian process by assuming conditional independence given neighborhood sets (Datta et al., 2016a,b,c). Let $\mathcal{S} = \{(\mathbf{s}_1, t_1), (\mathbf{s}_2, t_2), \dots, (\mathbf{s}_k, t_k)\}$ of k distinct location-time pairs denote the reference set, where we allow time to act as a natural ordering and impose an ordering on the locations observed at identical times. Then, we define neighborhood sets $N_{\mathcal{S}} = \{N(\mathbf{s}_i, t_i); i = 1, \dots, k\}$ over the reference set with $N(\mathbf{s}_i, t_i)$ consisting of the m nearest-neighbors of (\mathbf{s}_i, t_i) , selected from $\{(\mathbf{s}_1, t_1), (\mathbf{s}_2, t_2), \dots, (\mathbf{s}_{i-1}, t_{i-1})\}$. If $i \leq m + 1$, $N(\mathbf{s}_i, t_i) = \{(\mathbf{s}_1, t_1), (\mathbf{s}_2, t_2), \dots, (\mathbf{s}_{i-1}, t_{i-1})\}$.

Along with \mathcal{S} , $N_{\mathcal{S}}$ defines a Gaussian directed acyclic graph $\mathbf{w}_{\mathcal{S}}$ with a joint distribution

$$p(\mathbf{w}_{\mathcal{S}}) = \prod_{i=1}^k p(\mathbf{w}(\mathbf{s}_i, t_i) \mid \mathbf{w}_{N(\mathbf{s}_i)}) = \prod_{i=1}^k \mathcal{N}(\mathbf{w}(\mathbf{s}_i, t_i) \mid \mathbf{B}_{(\mathbf{s}_i, t_i)} \mathbf{w}_{N(\mathbf{s}_i, t_i)}, \mathbf{F}_{(\mathbf{s}_i, t_i)}), \quad (22)$$

where \mathcal{N} is a normal distribution,

$$\begin{aligned} \mathbf{B}_{\mathbf{s}_i, t_i} &= C_{(\mathbf{s}_i, t_i), N(\mathbf{s}_i, t_i)} C_{N(\mathbf{s}_i, t_i)}^{-1}, \\ \mathbf{F}_{(\mathbf{s}_i, t_i)} &= C((\mathbf{s}_i, t_i), (\mathbf{s}_i, t_i)) - \mathbf{B}_{(\mathbf{s}_i, t_i)} C_{N(\mathbf{s}_i, t_i), (\mathbf{s}_i, t_i)}, \end{aligned}$$

and $\mathbf{w}_{N(\mathbf{s}_i)}$ is the subset of $\mathbf{w}_{\mathcal{S}}$ corresponding to neighbors $N(\mathbf{s}_i)$ (Datta et al., 2016a). Datta et al. (2016a) extends this Gaussian DAG to a Gaussian process. This Gaussian process formulation only requires storage of $k m \times m$ distance matrices and requires many fewer floating point operations than full Gaussian process models (see Datta et al., 2016a). Like any other Gaussian process model, the nearest-neighbor Gaussian process can be utilized hierarchically for spatiotemporal random effects. In this article, we use nearest-neighbor Gaussian processes as an alternative to the full Gaussian process specification.

We envision our model taking the following form:

$$\begin{aligned} Y(\mathbf{s}, t) &= \mathbf{x}(\mathbf{s}, t)^\top \boldsymbol{\beta} + w(\mathbf{s}, t) + \epsilon(\mathbf{s}, t), \\ w(\mathbf{s}, t) &\sim \mathcal{N}(0, C((\mathbf{s}, t), (\mathbf{s}', t'))), \\ \epsilon(\mathbf{s}, t) &\stackrel{iid}{\sim} \mathcal{N}(0, \tau^2), \end{aligned} \quad (23)$$

where $Y(\mathbf{s}, t)$ is a spatiotemporal process measured (with error), $\mathbf{x}(\mathbf{s}, t)$ are spatiotemporal covariates. We define $C((\mathbf{s}, t), (\mathbf{s}', t'))$ using a covariance model discussed in Section 2 or Section 3. Lastly, we recommend using inverse gamma prior distributions for τ^2 from the pure error term and σ^2 from the covariance function because this selection gives closed form full conditional distributions. If the outcomes and covariates are centered, then an intercept is unnecessary. If covariates are not available, then $\mathbf{x}(\mathbf{s}, t)^\top \boldsymbol{\beta}$ is replaced with μ . The full conditional distributions for the Gibbs sampler, which we denote $\cdot \mid \dots$, are

$$\begin{aligned} \boldsymbol{\beta} \mid \dots &\sim \mathcal{N}(V_{\boldsymbol{\beta}}^* m_{\boldsymbol{\beta}}^*, V_{\boldsymbol{\beta}}^*) \\ \tau^2 \mid \dots &\sim IG(a_{\tau}^*, b_{\tau}^*) \end{aligned}$$

$$\begin{aligned}\sigma^2 &| \dots \sim IG(a_V^*, b_V^*) \\ \mathbf{w}_i &| \dots \sim \mathcal{N}(V_{w_i}^* m_{w_i}^*, V_{w_i}^*)\end{aligned}$$

where

$$\begin{aligned}V_\beta^* &= (\mathbf{X}^\top \mathbf{X} / \tau^2 + V_\beta^{-1})^{-1} \\ m_\beta^* &= V_\beta^{-1} m_\beta + \sum_i \mathbf{x}_i (y_i - w_i) / \tau^2 \\ V_{w_i}^* &= \left(1/\tau^2 + F_{s_i}^{-1} + \sum_{t:U(s_i)} B_{t,s_i}^\top F_t^{-1} B_{t,s_i} \right)^{-1} \\ m_{w_i}^* &= (y_i - \mathbf{x}_i^\top \boldsymbol{\beta}) / \tau^2 + F_{s_i}^{-1} B_{s_i} \mathbf{w}_{N(s_i)} + \sum_{t:U(s_i)} B_{t,s_i}^\top F_t^{-1} \mathbf{a}_{t,s_i} \\ a_V^* &= a_V + n/2 \\ b_V^* &= b_V + \sum_i (\mathbf{w}_i - B_{s_i} \mathbf{w}_{N(s_i)})^\top (\mathbf{w}_i - B_{s_i} \mathbf{w}_{N(s_i)}) / R_{s_i} \\ a_\tau^* &= a_\tau + \frac{n}{2} \\ b_\tau^* &= b_\tau + \frac{1}{2} \sum_i (y_i - \mathbf{x}_i^\top \boldsymbol{\beta} - w_i)^2,\end{aligned}$$

and \mathbf{a}_{t,s_i} is as it is defined in Datta et al. (2016a).

For prediction at an arbitrary location and time requires selection of m nearest-neighbors from the reference set \mathcal{S} for that location-time pair. We discuss two ways of selecting m neighbors. In theory, any location-time pair from the reference set can be selected as a neighbor for any prediction. If we allow predictions to depend on data occurring after the prediction time, then we call this a *retrospective* prediction since such a prediction could only be made retrospectively. On the other hand, a *prospective* prediction limits neighbor selection to elements of \mathcal{S} that occur at the same time or prior to the time of prediction. Datta et al. (2016c) selects neighbors for prospective predictions, and we do the same in our analyses.

Predicted spatiotemporal random effects at location-time pairs follow a conditional normal distribution, where conditioning is limited to its neighbors. For any space-time pair (\mathbf{s}, t) , the conditional distribution of the random effect is

$$\mathbf{w}(\mathbf{s}) | \mathbf{w}_{N(\mathbf{s})} \sim \mathcal{N} \left(C_{\mathbf{s}, N(\mathbf{s})} C_{N(\mathbf{s})}^{-1} \mathbf{w}_{N(\mathbf{s})}, C(\mathbf{s}, \mathbf{s}) - C_{\mathbf{s}, N(\mathbf{s})} C_{N(\mathbf{s})}^{-1} C_{\mathbf{s}, N(\mathbf{s})}^\top \right). \quad (24)$$

Then, the posterior prediction $Y(\mathbf{s}, t) \mid \mathbf{Y}$ is $\mathbf{x}(\mathbf{s}, t)^\top \boldsymbol{\beta} + w(\mathbf{s}, t) + \epsilon_i(\mathbf{s}, t)$, where, in practice, posterior samples of $\boldsymbol{\beta}$, $w(\mathbf{s}, t)$, and τ^2 are used to sample from the posterior predictive distribution. Predictions at held-out location-time pairs can be used to compare competing models.

Appendix 6

Simulation Study

In this simulation study, we generate a dataset from the following model:

$$\begin{aligned} Y(\mathbf{s}, t) &= w(\mathbf{s}, t) + \epsilon_i(\mathbf{s}, t), \\ w(\mathbf{s}, t) &\sim \text{GP}(0, C((\mathbf{s}, t), (\mathbf{s}', t'))), \\ \epsilon(\mathbf{s}, t) &\sim N(0, \tau^2), \end{aligned}$$

where observations lie on an evenly spaced grid of latitudes ranging from -90 to -60 (2.5° spacing) and longitudes between -180 and 0 (2.5° spacing). This grid is repeated from times 1 to 10, giving $N = 8780$. While we use a full Gaussian process specification for simulation, we fit these data using a hierarchical nearest-neighbor Gaussian process model with $m = 25$ neighbors. Neighbors are selected using simple rectangular neighborhood sets using great-circle (spherical) distance to define nearness (see Datta et al., 2016c). In addition to simulating over the regular grid, we simulate unobserved (held-out) data an additional 200 locations over the same time window, which gives us as a validation dataset of 2000. The generative covariance model comes from Equation 13 with $\sigma^2 = 4$, $c_s = 0.2$, $c_t = 2$, $\alpha = 1$, $\delta = 3/4$, $\gamma = 1/2$, and $\beta = 1/2$ and has $\tau^2 = 1$ for the noise term $\epsilon(\mathbf{s}, t)$.

For this simulation, we examine predictive performance of competing models and how well the model was able to estimate the parameters of the generative model. It should be noted that empirical model identifiability does not prove that all parameters are identifiable. Indeed many covariance models have limited parameter identifiability, for example the Matérn class is identifiable up to $\sigma^2 c_s^{-2\nu}$ (see Zhang, 2004). Thus, simulation results are only moderately informative.

For simplicity, we constrain $\delta + \beta/2 = 1$ for all models, $\gamma = 1/2$ for all models, and $\lambda = 1$ for Equations 12 and 14. For τ^2 and σ^2 , we use inverse-gamma priors with 0.1 as both the shape and rate parameters. We assume $c_s \sim \text{Unif}(0, \pi)$, $c_t \sim \text{Unif}(0, 10)$, $\alpha \sim \text{Unif}(0, 2]$, and $\beta \sim \text{Unif}(0, 1]$ *a priori*. A comparison between several covariance models using predictive measures is given in Table 7. With the exception of 90% empirical interval coverage, the true model (Equation 13) had the best predictive performance for all criteria (tied with Equation 12).

Equation	PRMSE	PMAE	90% Coverage	CRPS
(10) and $\nu = 1/2$	1.248	1.003	0.890	0.706
(10) and $\nu = 3/2$	1.249	1.005	0.879	0.707
(11)	1.219	0.982	0.897	0.690
(12)	1.217	0.980	0.895	0.688
(13)	1.217	0.980	0.894	0.688
(14)	1.218	0.981	0.895	0.689

Table 7: Predictive performance of competing covariance models. Highlights are used to indicate the generative model and best performers (i.e. lowest PRMSE, PMAE, and CRPS and 90% interval coverage closest to 90%).

Posterior summaries for the true model are given in Table 8. The 95% credible interval for

all covariance parameters contains the true value, indicating that the covariance model is, at least, empirically identifiable in this example.

	True Value	Mean	Std. Err.	C.I. 2.5%	C.I. 97.5%
τ^2	1	0.918	0.021	0.877	0.961
σ^2	4	4.299	0.405	3.582	5.109
c_s	0.2	0.172	0.017	0.142	0.209
c_t	2	1.784	0.320	1.279	2.489
α	1	0.966	0.096	0.785	1.173
β	0.5	0.505	0.269	0.043	0.962

Table 8: Posterior summaries for parameters for the model fit using Equation 13

Appendix 7

Locations of Hold-out Data from Section 5

Here, we provide the locations of held-out data used for model validation. The locations for held-out air temperature are given in Figure 5. The locations for held-out cloud coverage are in Figure 6.

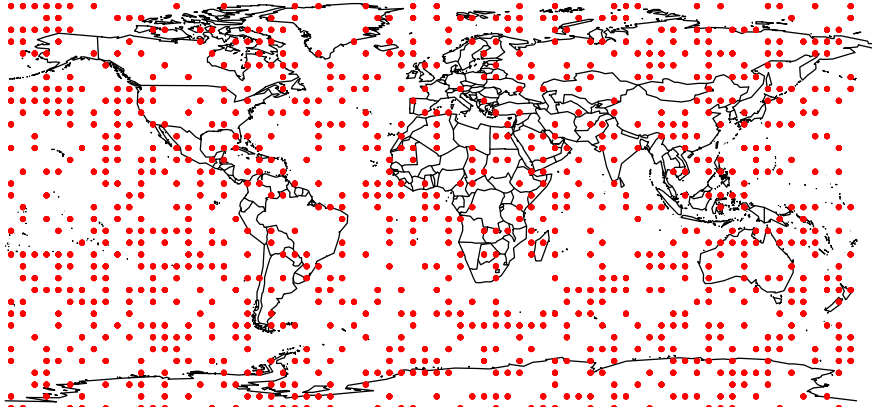


Figure 5: Hold-out locations used for predictive performance for the near-surface air temperature.

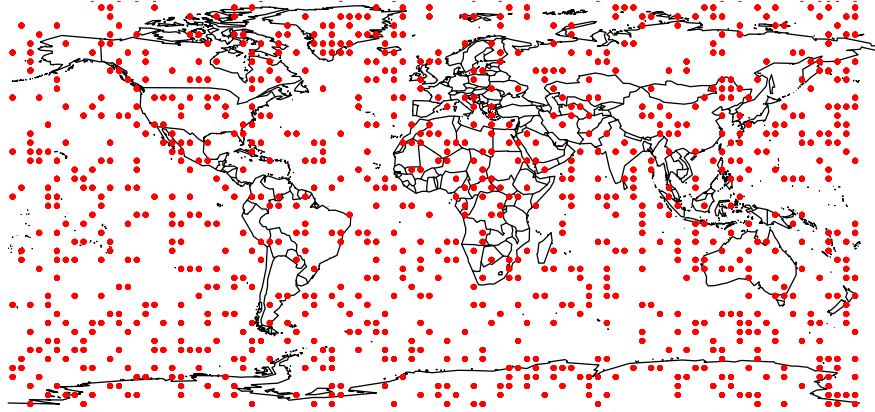


Figure 6: Hold-out locations used for predictive performance for the total cloud coverage dataset.

References

- ALEGRIA, A. & PORCU, E. (2017). The Dimple Problem related to Space-Time Modeling under the Lagrangian Framework. *Journal of Multivariate Analysis* **162**, 110–121.
- ALEGRIA, A., PORCU, E., FURRER, R. & MATEU, J. (2017). Covariance Functions for Multivariate Gaussian Fields Evolving Temporally over Planet Earth. *Technical Report, University Federico Santa Maria*.
- APANASOVICH, T. & GENTON, M. (2010). Cross-covariance functions for multivariate random fields based on latent dimensions. *Biometrika* **97**, 15–30.
- BANERJEE, S. (2005). On geodetic distance computations in spatial modeling. *Biometrics* **61**, 617–625.
- BANERJEE, S., CARLIN, B. P. & GELFAND, A. E. (2014). *Hierarchical modeling and analysis for spatial data*. Crc Press.
- BANERJEE, S., GELFAND, A. E., FINLEY, A. O. & SANG, H. (2008). Gaussian predictive process models for large spatial data sets. *Journal of the Royal Statistical Society: Series B (Statistical Methodology)* **70**, 825–848.
- BARBOSA, V. S. & MENEGATTO, V. A. (2017). Strict Positive Definiteness on Products of Compact Two-Point Homogeneous Spaces. *Integral Transforms Spec. Functions* **28**, 56–73.
- BATEMAN, H. (1954). *Tables of Integral Transforms, Volume I*. McGraw-Hill Book Company, New York.

- BERG, C. & PORCU, E. (2017). From Schoenberg Coefficients to Schoenberg Functions. *Constructive Approximation* **45**, 217–241.
- CASTRUCCIO, S. & STEIN, M. L. (2013). Global Space-Time Models for Climate Ensembles. *Ann. Appl. Statist.* **7**, 1593–1611.
- CRESSIE, N. & JOHANNESSON, G. (2008). Fixed rank kriging for very large spatial data sets. *Journal of the Royal Statistical Society: Series B (Statistical Methodology)* **70**, 209–226.
- DAI, F. & XU, Y. (2013). *Approximation Theory and Harmonic Analysis on Spheres and Balls*. Springer.
- DATTA, A., BANERJEE, S., FINLEY, A. O. & GELFAND, A. E. (2016a). Hierarchical nearest-neighbor gaussian process models for large geostatistical datasets. *Journal of the American Statistical Association* **111**, 800–812.
- DATTA, A., BANERJEE, S., FINLEY, A. O. & GELFAND, A. E. (2016b). On nearest-neighbor gaussian process models for massive spatial data. *Wiley Interdisciplinary Reviews: Computational Statistics* **8**, 162–171.
- DATTA, A., BANERJEE, S., FINLEY, A. O., HAMM, N. A. & SCHAAP, M. (2016c). Nonseparable dynamic nearest neighbor gaussian process models for large spatio-temporal data with an application to particulate matter analysis. *The Annals of Applied Statistics* **10**, 1286–1316.
- FOLLAND, C. K., RAYNER, N. A., BROWN, S., SMITH, T., SHEN, S., PARKER, D., MACADAM, I., JONES, P., JONES, R. N. & NICHOLLS, N. (2001). Global temperature change and its uncertainties since 1861. *Geophysical Research Letters* **28**, 2621–2624.
- FURRER, R., GENTON, M. G. & NYCHKA, D. (2006). Covariance tapering for interpolation of large spatial datasets. *Journal of Computational and Graphical Statistics* **15**, 502–523.
- FURRER, R., GENTON, M. G. & NYCHKA, D. (2012). Covariance tapering for interpolation of large spatial datasets. *Journal of Computational and Graphical Statistics* .
- GELMAN, A., CARLIN, J. B., STERN, H. S., DUNSON, D. B., VEHTARI, A. & RUBIN, D. B. (2014). *Bayesian data analysis*, vol. 2. CRC press Boca Raton, FL.
- GNEITING, T. (2002). Nonseparable, stationary covariance functions for space–time data. *Journal of the American Statistical Association* **97**, 590–600.
- GNEITING, T. (2013). Strictly and non-strictly positive definite functions on spheres. *Bernoulli* **19**, 1327–1349.
- GNEITING, T. & RAFTERY, A. E. (2007). Strictly proper scoring rules, prediction, and estimation. *Journal of the American Statistical Association* **102**, 359–378.
- GNEITING, T. & SCHLATHER, M. (2004). Stochastic models that separate fractal dimension and the hurst effect. *SIAM Rev.* **46**, 269–282.

- GRADSHTEYN, I. S. & RYZHIK, I. M. (2007). *Tables of Integrals, Series, and Products*. Academic Press, Amsterdam, seventh ed.
- GRAMACY, R. B. & APLEY, D. W. (2015). Local gaussian process approximation for large computer experiments. *Journal of Computational and Graphical Statistics* **24**, 561–578.
- GUELLA, J. C., MENEGATTO, V. A. & PERON, A. P. (2016a). An Extension of a Theorem of Schoenberg to a Product of Spheres. *Banach J. Math. Anal.* **10**, 671–685.
- GUELLA, J. C., MENEGATTO, V. A. & PERON, A. P. (2016b). Strictly Positive Definite Kernels on a Product of Spheres ii. *SIGMA* **12**.
- GUELLA, J. C., MENEGATTO, V. A. & PERON, A. P. (2017). Strictly Positive Definite Kernels on a Product of Circles. *Positivity* **21**, 329–342.
- HANSEN, J., RUEDY, R., SATO, M. & LO, K. (2010). Global surface temperature change. *Reviews of Geophysics* **48**.
- HANSEN, J., SATO, M., RUEDY, R., LO, K., LEA, D. W. & MEDINA-ELIZADE, M. (2006). Global temperature change. *Proceedings of the National Academy of Sciences* **103**, 14288–14293.
- HEATON, M. J., DATTA, A., FINLEY, A., FURRER, R., GUHANIYOGI, R., GERBER, F., GRAMACY, R. B., HAMMERLING, D., KATZFUSS, M. & LINDGREN, F. (2017). Methods for analyzing large spatial data: A review and comparison. *arXiv preprint arXiv:1710.05013*.
- HEINE, V. (1955). Models for two-dimensional stationary stochastic processes. *Biometrika* **42**, 170–178.
- HELD, I. M. & SODEN, B. J. (2006). Robust responses of the hydrological cycle to global warming. *Journal of climate* **19**, 5686–5699.
- HIGDON, D. (2002). Space and space-time modeling using process convolutions. In *Quantitative methods for current environmental issues*. Springer, pp. 37–56.
- JEONG, J. & JUN, M. (2015). A Class of Matern-like Covariance Functions for Smooth Processes on a Sphere. *Spatial Statistics* **11**, 1–18.
- KALNAY, E., KANAMITSU, M., KISTLER, R., COLLINS, W., DEAVEN, D., GANDIN, L., IREDELL, M., SAHA, S., WHITE, G. & WOOLLEN, J. (1996). The ncep/ncar 40-year reanalysis project. *Bulletin of the American meteorological Society* **77**, 437–471.
- KAUFMAN, C. G., SCHERVISH, M. J. & NYCHKA, D. W. (2008). Covariance tapering for likelihood-based estimation in large spatial data sets. *Journal of the American Statistical Association* **103**, 1545–1555.
- MELILLO, J. M., MCGUIRE, A. D., KICKLIGHTER, D. W., MOORE, B., VOROSMARTY, C. J. & SCHLOSS, A. L. (1993). Global climate change and terrestrial net primary production. *Nature* **363**, 234.

- PARMESAN, C. & YOHE, G. (2003). A globally coherent fingerprint of climate change impacts across natural systems. *Nature* **421**, 37.
- PORCU, E., ALEGRÍA, A. & FURRER, R. (2018). Modeling temporally evolving and spatially globally dependent data. *International Statistical Review* **To Appear**.
- PORCU, E., BEVILACQUA, M. & GENTON, M. G. (2016). Spatio-Temporal Covariance and Cross-Covariance Functions of the Great Circle Distance on a Sphere. *Journal of the American Statistical Association* **111**, 888–898.
- PORCU, E., GREGORI, P. & MATEU, J. (2006). Nonseparable stationary anisotropic space–time covariance functions. *Stochastic Environmental Research and Risk Assessment* **21**, 113–122.
- PORCU, E., MATEU, J. & BEVILACQUA, M. (2007). Covariance Functions which are Stationary or Nonstationary in Space and Stationary in Time. *Statistica Neerlandica* **61**, 358–382.
- PORCU, E., MATEU, J. & CHRISTAKOS, G. (2010). Quasi-Arithmetic Means of Covariance Functions with Potential Applications to Space-Time Data. *J. Multivariate Anal.* **100**, 1830–1844.
- POUNDS, J. A., FOGDEN, M. P. & CAMPBELL, J. H. (1999). Biological response to climate change on a tropical mountain. *Nature* **398**, 611.
- RUE, H., MARTINO, S. & CHOPIN, N. (2009). Approximate bayesian inference for latent gaussian models by using integrated nested laplace approximations. *Journal of the royal statistical society: Series b (statistical methodology)* **71**, 319–392.
- SCHLATHER, M. (2010). Some Covariance Models based on Normal Scale Mixtures. *Bernoulli* **16**, 780–797.
- SCHOENBERG, I. J. (1938). Metric Spaces and Completely Monotone Functions. *Annals of Mathematics* **25**, 811–841.
- SCHOENBERG, I. J. (1942). Positive Definite Functions on Spheres. *Duke Math. Journal* **9**, 96–108.
- SIMMONS, A., JONES, P., DA COSTA BECHTOLD, V., BELJAARS, A., KÅLLBERG, P., SAARINEN, S., UPPALA, S., VITERBO, P. & WEDI, N. (2004). Comparison of trends and low-frequency variability in cru, era-40, and ncep/ncar analyses of surface air temperature. *Journal of Geophysical Research: Atmospheres* **109**.
- STEIN, M. L. (1999). *Statistical Interpolation of Spatial Data: Some Theory for Kriging*. Springer, New York.
- STEIN, M. L. (2008). A modeling approach for large spatial datasets. *Journal of the Korean Statistical Society* **37**, 3–10.
- STEIN, M. L. (2014). Limitations on low rank approximations for covariance matrices of spatial data. *Spatial Statistics* **8**, 1–19.

- STEIN, M. L., CHI, Z. & WELTY, L. J. (2004). Approximating likelihoods for large spatial data sets. *Journal of the Royal Statistical Society: Series B (Statistical Methodology)* **66**, 275–296.
- SVENSMARK, H. & FRIIS-CHRISTENSEN, E. (1997). Variation of cosmic ray flux and global cloud coveragea missing link in solar-climate relationships. *Journal of atmospheric and solar-terrestrial physics* **59**, 1225–1232.
- THOMAS, C. D., CAMERON, A., GREEN, R. E., BAKKENES, M., BEAUMONT, L. J., COLLINGHAM, Y. C., ERASMUS, B. F., DE SIQUEIRA, M. F., GRAINGER, A. & HANNAH, L. (2004). Extinction risk from climate change. *Nature* **427**, 145.
- VECCHIA, A. V. (1988). Estimation and model identification for continuous spatial processes. *Journal of the Royal Statistical Society. Series B (Methodological)* , 297–312.
- WYLIE, D., JACKSON, D. L., MENZEL, W. P. & BATES, J. J. (2005). Trends in global cloud cover in two decades of hirs observations. *Journal of climate* **18**, 3021–3031.
- ZHANG, H. (2004). Inconsistent estimation and asymptotically equal interpolations in model-based geostatistics. *Journal of the American Statistical Association* **99**, 250–261.